J Electroceram (2010) 25:179–187
DOI 10.1007/s10832-010-9613-8

Low-temperature sintering of $BaTiO_3$ with Mn-Si-O glass

Jerry C. C. Lin · Wen-Cheng J. Wei

Received: 4 March 2009 / Accepted: 21 May 2010 / Published online: 8 June 2010

Abstract In order to reduce sintering temperature and prevent adverse dielectric effects, pure $BaTiO_3$ powder with the addition of Mn-Si-O glass was sintered in the temperature range of 1175–1300°C. Microstructural observation showed that $BaTiO_3$ grains of the sintered samples only grew from the initial 400 nm to an average of 430 nm between 1175–1275°C for 1 h, or sintered at 1250°C as long as 27 h. Abnormal $BaTiO_3$ grains are not found in the sintered samples. The microstructure and phase analysis showed that the dielectric properties, tetragonality, and grain growth of $BaTiO_3$ are closely controlled by the formation of the liquid phase, newly formed $Ba_2TiSi_2O_8$ grains, and Mn solid solution in $BaTiO_3$ grains.

Keywords $BaTiO_3 \cdot$ Sintering $\cdot Mn_2O_3 \cdot SiO_2$

1 Introduction

Liquid phase sintering has been one of the critical challenges in MLCC technologies in past decade. Glass phase usually segregates to grain boundaries and degrades the dielectric properties of the ceramic device [1–3]. In some cases, the addition of sintering aids can not only contribute to the formation of liquid phase, but also enhance $BaTiO_3$ exaggerated grain growth in the dielectric layer by lower temperature sintering [4, 5]. Besides, the liquid phase offers a route for quick diffusion of various dopants [6, 7].

J. C. C. Lin · W.-C. J. Wei (✉)
Institute of Materials Science and Engineering,
National Taiwan University,
Taipei, Taiwan
e-mail: wjwei@ntu.edu.tw

SiO_2 is a glass former which is able to be alloyed with manganese (Mn) oxide to form eutectic liquid at ~1200°C. In addition, using Mn as the electron trapper in reducing sintering of base-metal-electrode (BME) capacitor is a well-known method. The valence state of Mn changes according to the oxidation condition, and the ions offer good atomic site on electron trapping as the reaction shown below [8].

$$Mn_{Ti} + ne^- \rightarrow Mn_{Ti}^{n-} \quad (1)$$

Mn ions offer the valence transition to balance free electrons from the donation of the oxygen vacancy of $BaTiO_3$ by reducing sintering [9].

$$Null_{BT} \rightarrow V_0^{2+} + 2e^- \quad (2)$$

Temperature flattening characteristics (TFC) of $BaTiO_3$ after extra element doping is also critical to the applications of multi-layer capacitors (MLCs). The X7R case with capacitance variation ($\Delta C/C$) in ±15% between −55 ~ 125°C is usually resulted by the formation of core-shell structure of $BaTiO_3$ grains [10–12]. The shell part appears cubic-phase, which is resulted from the substitution of Ba^{2+} or Ti^{4+} sites (also called "A and B" sites) by doping elements, for instance Mg, Y, Ho, etc [13, 14]. The core part shows tetragonal structure, where fewer or no solid solution is resulted. Due to small amount of Mn ion being added to $BaTiO_3$, the Mn content is difficult to be detected. Therefore, solid-solution of Mn ion into $BaTiO_3$ is also discussed in this study by different characterization techniques.

In order to lower the sintering temperature and minimize the grain size of $BaTiO_3$, one kind of glassy powder in one composition of Mn-Si-O eutectics was investigated to resolve the reactions at interface and the microstructure evolution at temperatures above 1050°C. Following the previous study [15], the glass is employed as a sintering aid in this study. The

objective of this work is to investigate the effects of Mn-Si-O glass on the sintering of $BaTiO_3$. This paper will critically examine the evolution of densification and growth processes, and relate these results to presence of the liquid phase and any secondary phases. Lastly, the paper will examine the relation of these processes and the presence of second phases to the dielectric performance of the ceramic material.

2 Experimental procedures

2.1 Sample preparation

1.5 Mn_2O_3-2SiO_2 powder mixture was melted at 1400°C for 1 h and then cooled in water to produce the glass frits. Glass powder was ground by high-purity Al_2O_3 mortar and pestle and passed the screen of 200 mesh. The ground glass powder was added into $BaTiO_3$ (Yageo Corp., Taiwan, A/B=1.000 with an average particle size of 0.40 μm) which was mixed in aqueous solution (pH=~10.5, controlled by ammonia) with a small amount of dispersant. After ball milling for 24 h, green disks were formed by pressure casting, called "PC-BT". The other samples prepared with various amounts of the glass addition were die-pressed at the pressure of 100 MPa, called "DP-BT". The detail procedures for the preparation of DP-BT sample are described as below. $BaTiO_3$ powder was first mixed with various amounts of the glass (0.1~3.0 wt%) in ethanol by ball milling for 24 h. After dried in an oven, the dried powder was ground and then sieved through 200 meshes before die-pressing. The power (0.20 g) was uni-axially pressed into a disk of 6.0 mm in diameter and 2.5~3.0 mm in thickness. Green samples, DP- and PC-BT, were sintered at 1100~1300°C for various durations in air.

2.2 Property measurements

The sintering behavior of glass-added BT was analyzed by using a thermo-mechanical analyzer (TMA, SETSYS TMA 16/18, SETRAM Co., France). Sintered density of the samples was measured by Archimedes' method, and the theoretical density of each sample was calculated based on the theoretical density (T.D.) of $BaTiO_3$ (5.87 g/cm^3) and the as-prepared Mn-Si-O glass (3.87 g/cm^3, by Accu Pyc 1330, Micromeritics, USA). Two dielectric properties, including dielectric constant (k) and dielectric loss (tanδ) of sintered $BaTiO_3$ disks were measured. Ag paste was painted on each side of the sintered disks, and served as electrodes. The condition of 600°C for 1 h with a heating rate of 1°C/min was used to bake the painted samples. Finally, the dielectric constant and dielectric loss were both measured by an impedance analyzer, (6420, Wayne Kerr, England) under 1 V, 1 kHz.

Variation of the lattice parameters (tetragonality = c/a) of sintered BT was studied by X-ray diffractometry (Philips PW 1972, Philips Instrument, Netherlands) using Cu K_α radiation. The peaks in XRD spectrum were best fitted and analyzed by the software of Jade-5 and Cell-Parameter to get precise lattice parameters (a and c lattice constants).

The polished and thermally etched $BaTiO_3$ sintered samples were observed by SEM equipped with EDS (SEM 1530, Leo Co., Netherlands). A detailed microstructure analysis was completed using transmission electron microscopy (TEM 100CX, JEOL Co., Japan) and TEM equipped with EDS (FEG-TEM, Tecnai G2F20, Philips Co., USA). The average grain size of BT was measured by using the linear intercept technique from SEM and TEM micrographs.

3 Results

3.1 Sintering behavior of glass-added PC-BT

The shrinkage behavior of two samples, pure BT and 1 wt% glass-added PC-BT, is shown in Fig. 1(a). The onset temperature of the sintering of the samples is 1020°C and 1080°C, respectively. The higher onset temperature of the glass-added sample was probably caused by the expansion of glass phase in $BaTiO_3$ disk coming from the melting of the glass and the dissolution of $BaTiO_3$ into the glass [15]. The dynamic shrinkage curve of 1 wt% glass-added PC-BT exhibits multiple maximum shrinkage rates, which could be partially resulted from the compositional variation of liquid phase or formation of crystalline phases during heating [16]. The maximum densification rate of the glass-added sample occurred at ~1175°C, lower than that of pure $BaTiO_3$. This implies that some of the glass had become liquid wetting on $BaTiO_3$ particles at 1175°C.

Figure 1(b) shows the results of sintered density and average grain size of the PC-BT disks. Noticeable densification of the sample started around the temperature of 1100~1150°C and full densification was achieved at ≥1200°C. The average grain size of $BaTiO_3$ changed from the initial 400 nm to an average of 430 nm after sintering at 1250°C, showing slightly grain growth with this liquid phase. The standard deviation of the grain size is ~220 nm.

The microstructural observation of the sintered PC-BT disks is shown in Fig. 2. The glassy/particle aggregate, as shown in the center part of Fig. 2(a), is randomly distributed on the polished cross-section of the PC-BT sintered at 1050°C. The liquid at that temperature drags $BaTiO_3$ grains closer and gradually penetrates into pore channels, resulting in a decrease in porosity (Fig. 2(b)). Smaller pores could lead to a greater capillary force to liquid phase and induce deeper penetration. Full densification of the disk was achieved at 1200°C (Fig. 2(c)).

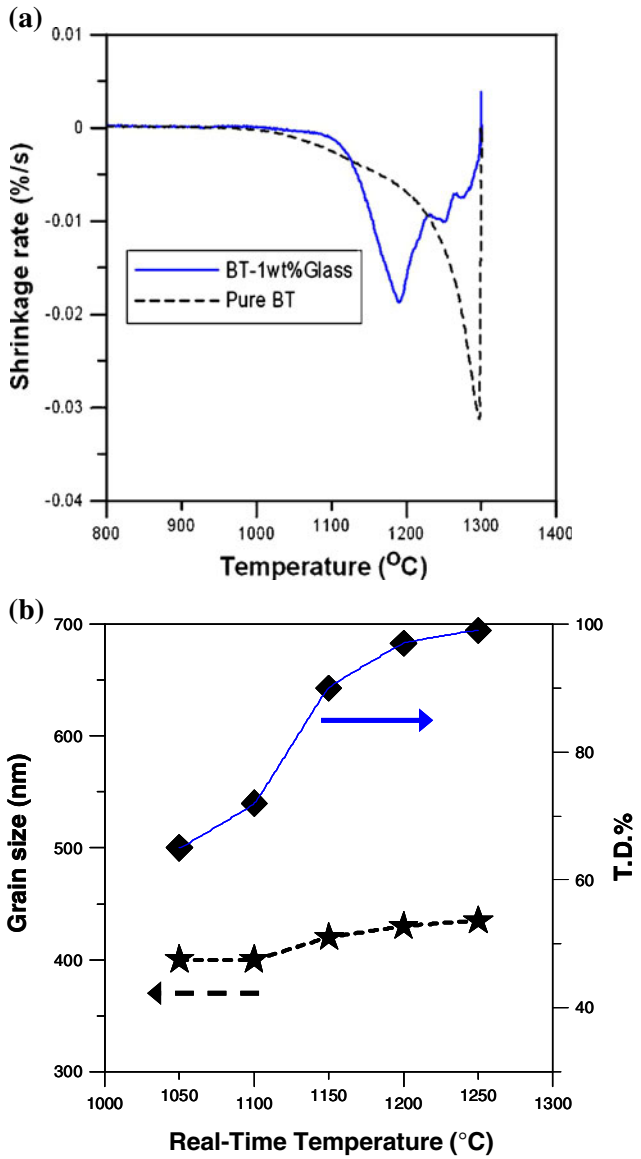

Fig. 1 (**a**) Shrinkage-rate curves of pure $BaTiO_3$ and 1 wt% glass-added PC-BT plotted against sintering temperature. (**b**) Sintered density and average grain size of 1 wt% glass-added PC-BT as a function of sintering temperature without holding time

3.2 Microstructure development

Average grain sizes of glass-added BT after sintering at different temperatures for 1 h are summarized in Fig. 3(a). The sintered density of the PC-BT achieved more than 95% T.D. when sintered at temperatures of 1175°C ~ 1275°C for 1 h. The average grain size of all BT samples was 430 nm in a standard deviation of ±220 nm, which is slightly bigger than the average particle size of as-received BT powder. After sintering at 1300°C, the average grain size of the sample abruptly grew to 60 μm, which was 3 times greater than that of pure BT. In order to reveal the effect of holding time on BT grain size, the PC-BT disks were also sintered

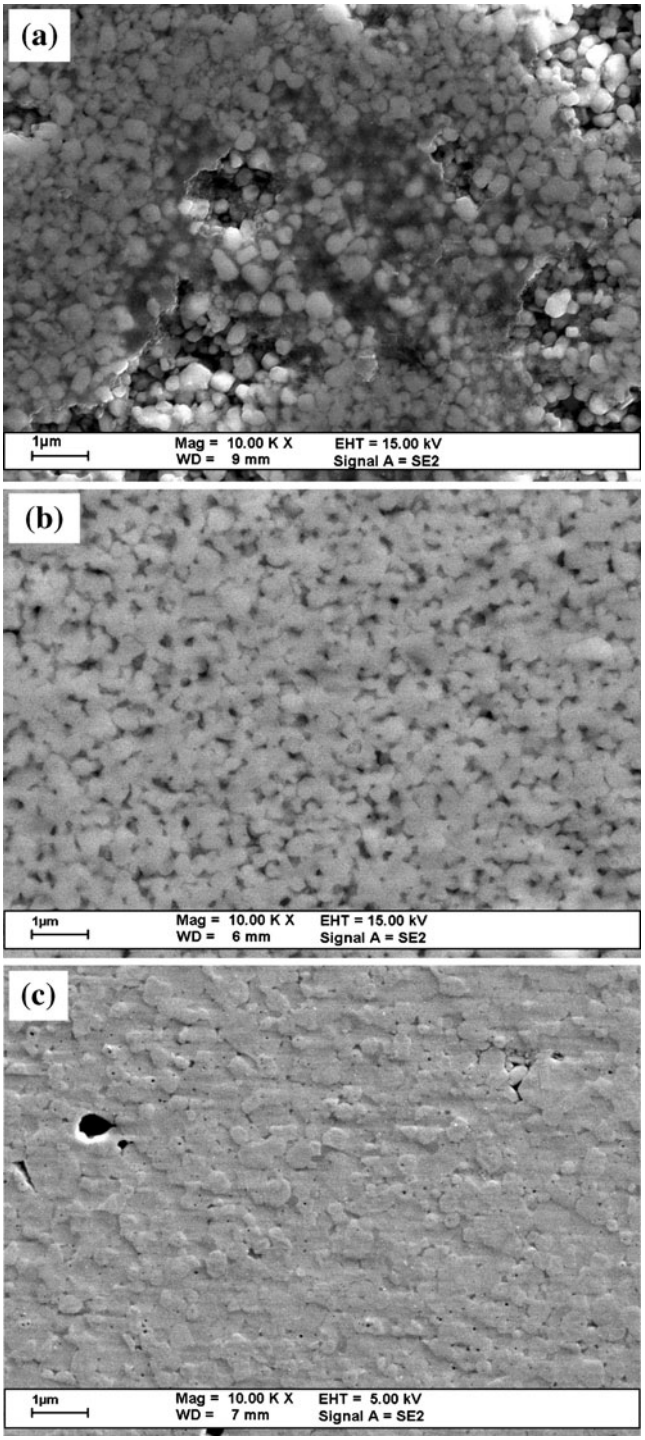

Fig. 2 SE images showing the morphologies of 1 wt% glass-added PC-BT at various temperatures without holding time. (**a**) The viscous phase at center composed of Ba-Ti-Si-O by 1050°C, (**b**) connected pores gradually disappearing at 1150°C, (c) achieving full density at 1200°C

at 1250°C holding for 1 h to 27 h. The grain sizes were measured and shown in Fig. 3(b). The average grain sizes of these BT samples were slightly grown from 400 nm to 430 nm during annealing process.

In general, the grain growth of $BaTiO_3$ ceramics in the final stage of sintering might follow diffusional-control or the other mechanism [17]. However, no grain growth was observed in this study after long sintering time. The alternative effects, either solute drag effect and/or second phase pinning effect possibly inhibits the grain growth. The factors will be discussed later.

One typical porous sample (1 wt% glass-added PC-BT sintered at 1125°C for 1 h) still remained about 20% porosity and analyzed by TEM with EDS. The images and EDS spectrum are shown in Figs. 4(a) and (b), respectively. The glassy layers as pointed out in the micrograph either cover $BaTiO_3$ grains or is located between BT grains. The composition of the glass included Si, Ba, Ti and O as detected by windowless EDS. The composition implied that $BaTiO_3$ dissolves into the glass during heating process. This new glass would reduce its melting temperature and benefit the densification at lower sintering temperature.

The disks of 1 wt% glass-added PC-BT and pure BT sintered at 1250°C for 1 h had different grain features, as shown in Figs. 5(a) and (b), respectively. The average grain size of the PC-BT sample with 1 wt% glass was close to 430 nm, and some grains shows twin features. In addition, few enclosed pores could be found inside $BaTiO_3$ grains. However, obvious grain growth of sintered pure $BaTiO_3$ grains occurred during the final stage of sintering, and the average grain size grew to 1.1 μm with no intragranular porosity observed.

From the magnified TEM BF image (Fig. 6(a)) of 1 wt% glass-added PC-BT, the second phases located at triple junctions were observed and pointed out in the micrograph. The crystalline phase can be identified as $Ba_2TiSi_2O_8$ by attached EDS spectrum and lattice image, as shown in Figs. 6(b) and (c), respectively. The $Ba_2TiSi_2O_8$ in Fig. 6(a) is possibly a liquid region during the sintering temperatures. The curved boundary of the neighbor $BaTiO_3$ grains to the $Ba_2TiSi_2O_8$ is the evidence of crystallization of a liquid. The convex boundary of $BaTiO_3$ next to the triple junction

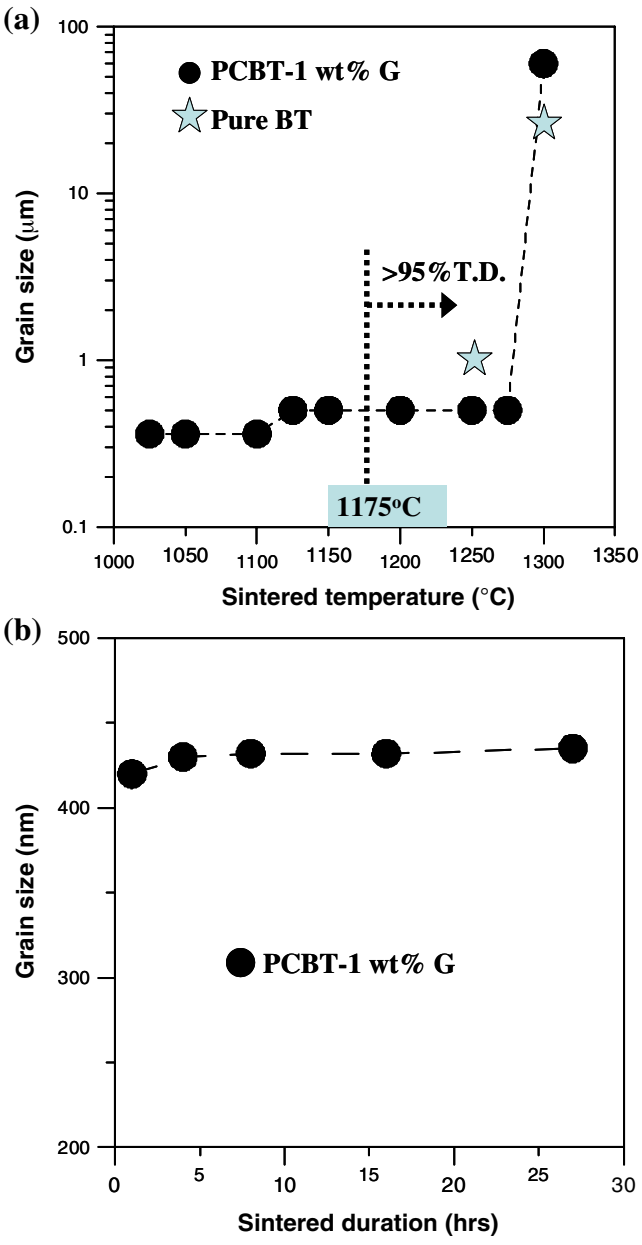

Fig. 3 Sintering profiles showing the relationship of average grain size vs. sintered temperature (**a**) of pure BT and 1 wt% glass added PC-BT after 1 h heating. The 1 wt% glass-added PC-BT could be densified to 95% T.D. at 1175°C for 1 h. (**b**) Average grain size of 1 wt% glass-added PC-BT during 27 h heated at 1250°C

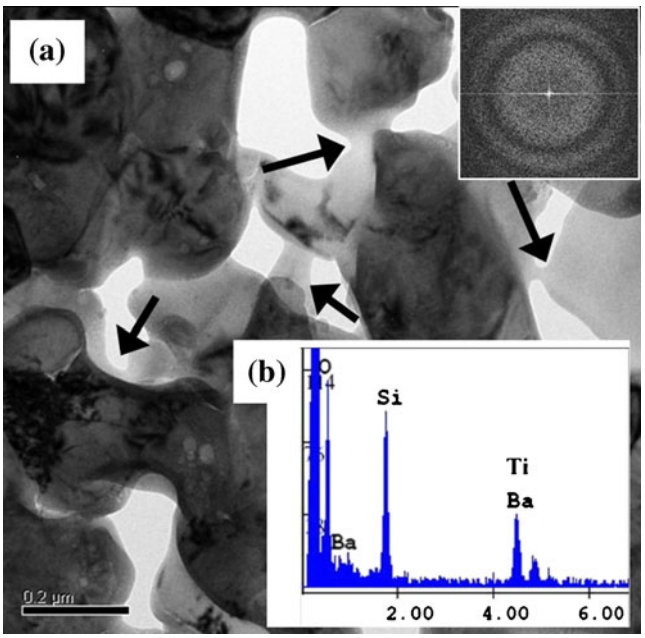

Fig. 4 (**a**) TEM BF image of 1 wt% glass-added PC-BT sintered at 1125°C for 1 h showing the glassy phase, pointed by black arrows and Fourier transform pattern (FTP) as the insert. (**b**) EDS result showing the composition of the glassy parts (Ba-Ti-Si-O)

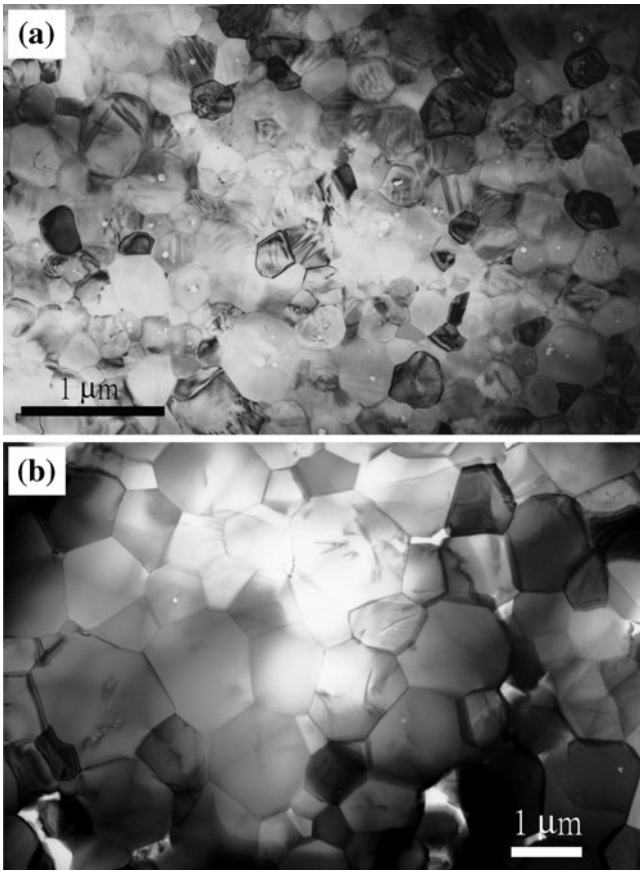

Fig. 5 TEM BF images showing the grain size distribution of (**a**) 1 wt % glass-added (**b**) pure PC-BT sintered at 1250°C for 1 h

implies that partial dissolution of the $BaTiO_3$ grains into the glassy has occurred during sintering.

Compositional analysis by TEM/EDS line scan was carried out to reveal the distribution of Mn element. The scanned region is marked in Fig. 7(a). Mn signal was detected showing a very low level and randomly distributed inside $BaTiO_3$ grain and at grain boundary (Fig. 7(b)). This result implies no segregation of Mn ion at the grain boundaries.

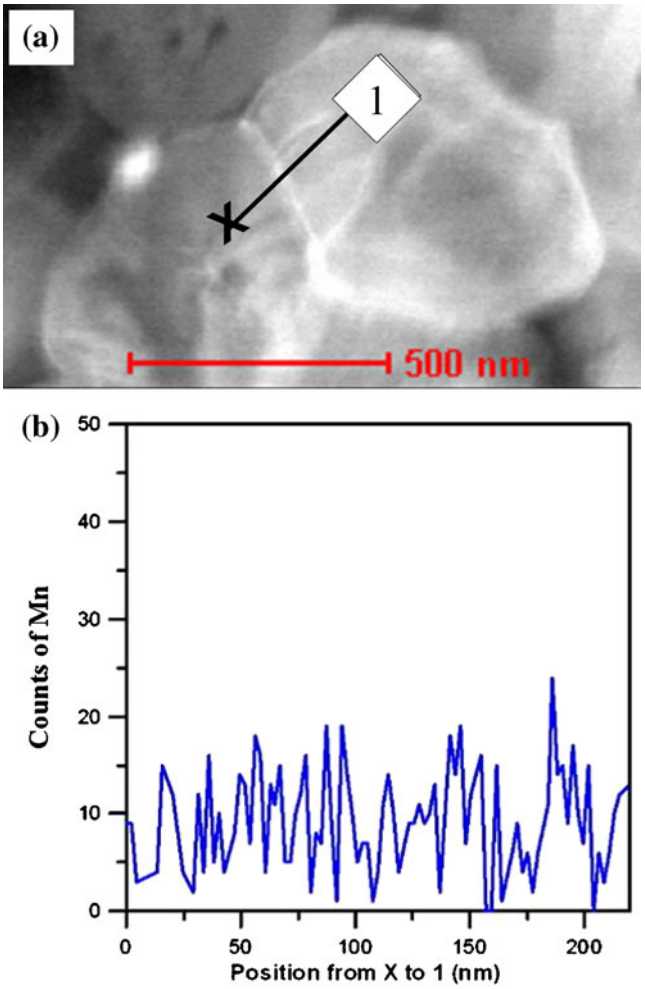

Fig. 7 (**a**) Scanning TEM image of 1 wt% glass-added PC-BT after heating at 1250°C for 1 h. (**b**) Analytical results by EDS-line scan showing no obvious Mn signal could be found across the grain boundary

In order to find additional evidence on solid solution of either Mn or Si on crystalline $BaTiO_3$, quantitative XRD analysis was conducted to determine the tetragonality, c/a, of various samples. Figure 8(a) shows the tetragonality of 1 wt%

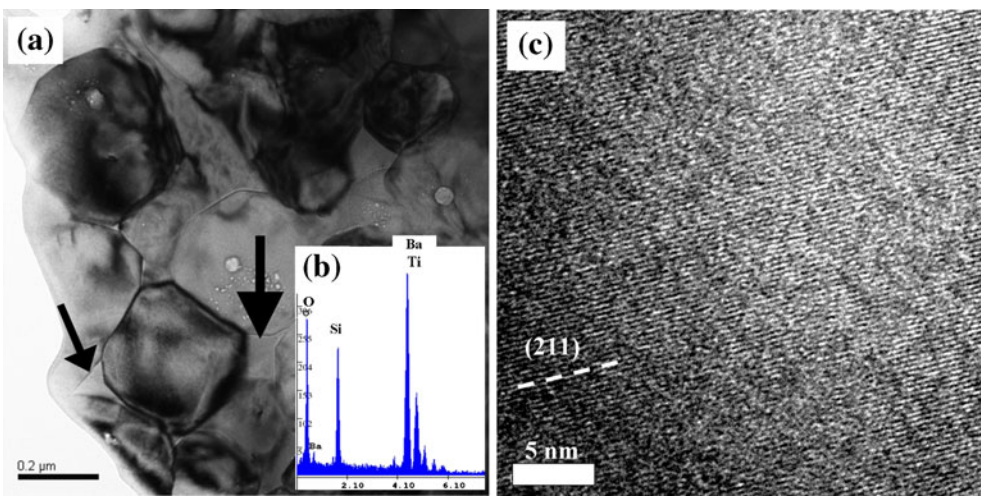

Fig. 6 (**a**) TEM BF, (**b**) EDS analysis showing the composition of the second phase being $Ba_2TiSi_2O_8$, and (**c**) HRTEM images showing the crystalline second phase (marked by black arrows in (a)), located at the triple junction of BT grains and some enclosed pores inside $BaTiO_3$ grains in the 1 wt% glass-added sample

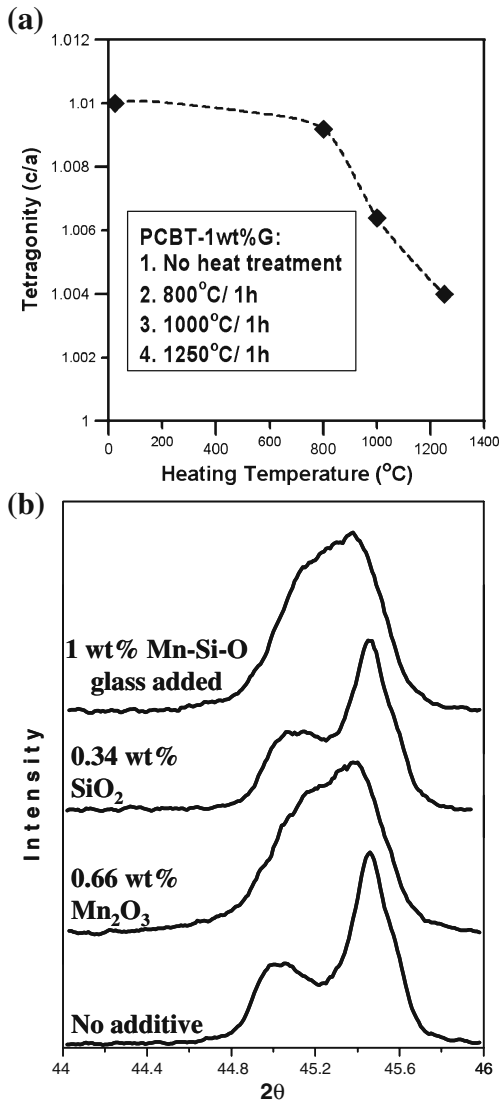

Fig. 8 (**a**) Quantitative XRD results showing the change of tetragonality of 1 wt% glass-added PC-BT after heating at different temperatures. (**b**) XRD spectra showing the peak shift in 1250°C/1 h heated samples due to solid-solution by Mn

glass added PC-BT decreases from 1.010 to 1.004 with temperatures from room temperature to 1250°C. The tetragonality of $BaTiO_3$ changes slightly to 1.009 after heated at 800°C and apparently to 1.004 at 1250°C.

Mn and Si elements have different degrees of influence on the tetragonality of $BaTiO_3$. XRD spectra of either 0.34 wt% SiO_2- or 0.66 wt/% Mn_2O_3-added BT samples were compared with that of 1 wt% glass-added and pure BT disks, as shown in Fig. 8(b). All of these samples had been sintered at 1250°C for 1 h. After differentiating these samples, diffraction peaks of (002) and (200) locating at 2θ between 44.8°–45.8° show that peaks shift was contributed by only Mn ion in solid-solution into $BaTiO_3$. Comparing the ionic radii of Si^{4+}, Mn^{2+}, Mn^{3+}, Ba^{2+}, and Ti^{4+} [15], Mn^{2+} or Mn^{3+} is suitable to substitute Ti^{4+}. The substitution $\left(Mn_{Ti}^{1-}\text{-}or\text{-}Mn_{Ti}^{2-}\right)$ reduces the tetragonality. Si ion seems too small to replace both A and B sites of BT.

3.3 Effects of glass content

Sintering behavior of 0–3.0 wt% glass to $BaTiO_3$ is shown by the shrinkage curves in Fig. 9(a). The glass-added samples have higher (30–100°C) onset of the sintering trend than that of the pure BT. The possible volume swelling [15], due to the dissolution of BT into Mn-Si-O glass, might dominate the onset of the sintering as opposed to liquid phase sintering and particle rearrangement at the initial stage. After more glass added to BT (~3.0 wt%), the onset of the sintering gradually came closer to that of the pure sample, which means more liquid phase was formed, providing enough quantity for

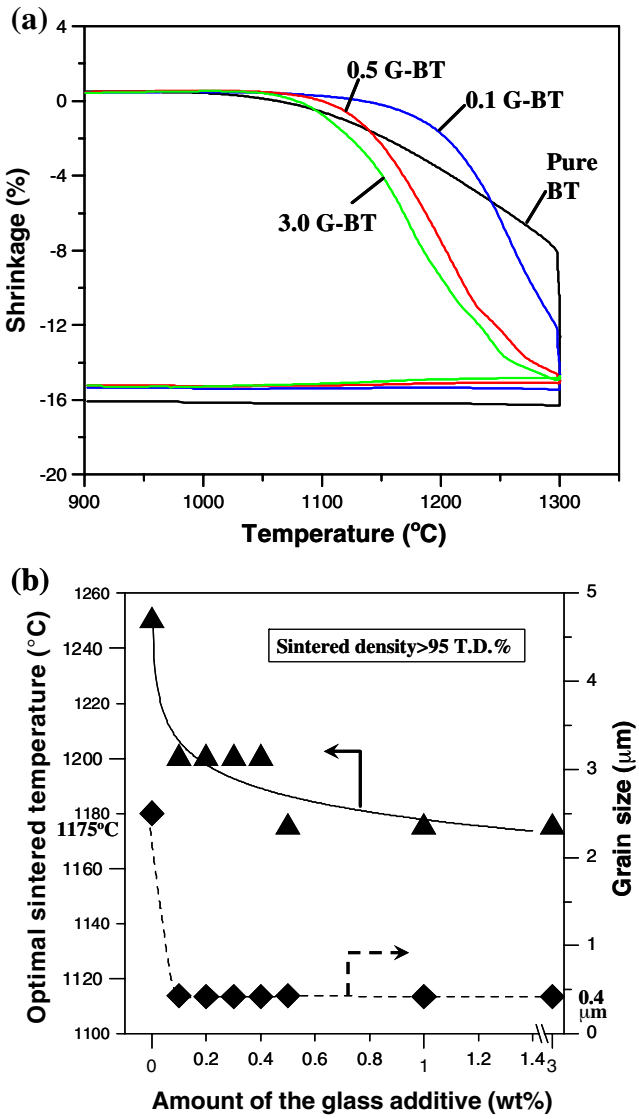

Fig. 9 (**a**) Shrinkage curves of glass-added $BaTiO_3$ samples. (**b**) The optimal sintering temperature and the corresponding average grain size of each sample

densification. When the glass content increased to 3 wt%, the onset of the sintering was dominated by liquid phase sintering, and shows larger shrinkage than that of pure BT. Optimal sintering temperature (the lowest temperature able to densify samples to >95% T.D. in 1 h) of various amounts of added glass are shown in Fig. 9(b). The 0.1~0.4 wt% glass addition leads to a reduction of sintering temperature to 1200°C, and 0.5~3.0 wt% glass additions can further reduce it to 1175°C.

Sintered density and grain size analysis of the glass-added $BaTiO_3$ by 1250°C treatment are shown in Fig. 10 (a). All samples kept a nearly constant grain size (430 nm) with the glass addition of 0.2 wt%, of which the glass addition contributes to grain growth inhibition. In Fig. 10 (b), the tetragonality remained at lowest level (1.004) when ≥0.5 wt% glass is added, implying that maximal solubility (about 1 mol%) of Mn in $BaTiO_3$ has been achieved.

Figure 11 shows the effect of glass addition on dielectric constant (k) and dielectric loss of sintered $BaTiO_3$. The dielectric constant is enhanced to 2200 by the 0.1 wt% glass addition. When the glass addition gets over than 0.1 wt%, k gradually decreases to the value of 1000. The dielectric loss (tanδ) changes to 0.01 as 0.1 wt% glass is added. When >0.1 wt% glass is added, the dielectric loss increases with the amount of glass addition.

4 Discussion

4.1 Mechanism of gain growth inhibition

Densification of glass-added BT involves the dissolution of BT particles into the glass and smaller particles lead to higher dissolution concentration into Mn-Si-O glass. In the early stage of densification, the dissolution of Ba and Ti ions occurs and helps reduce the melting point of the glass. The composition of the liquid phase changes during heating. The glass also offers a fast diffusion route for dissolution-precipitation process. The glass contributes to particle rearrangement by capillarity force, which is also beneficial to the densification of the $BaTiO_3$ disks. The liquid phase, which has good wet-ability on BT powders, plays an important role in densification.

During the heating process, Mn ions in the liquid rapidly dissolve into the $BaTiO_3$ grains, the remaining liquid finally

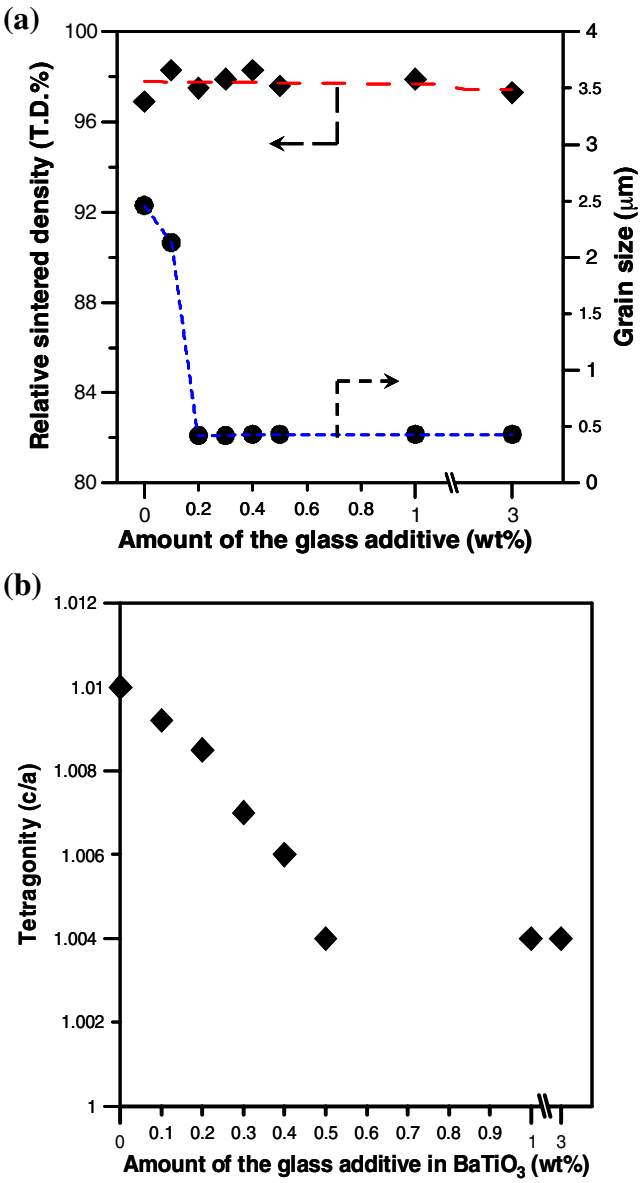

Fig. 10 (**a**) Sintered densities and average grain sizes, (**b**) quantitative tetragonality (c/a) results of $BaTiO_3$ via various amounts of glass addition after sintering at 1250°C for 1 h

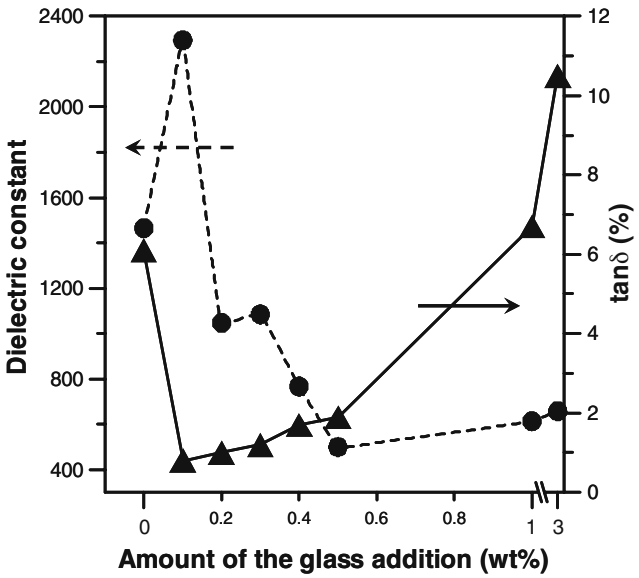

Fig. 11 Effects of the glass addition on dielectric constant and dielectric loss of $BaTiO_3$ disks after sintered at 1250°C for 1 h in air atmosphere

crystallizes as the composition runs out of Mn content, resulting in crystallization of $Ba_2TiSi_2O_8$ phase at triple junction (Fig. 6). The grain boundary phase has potential to inhibit grain growth of $BaTiO_3$ grains by pinning effect in final stage of sintering [18]. The reactions can be described as follows if all Mn ions can solid-solute into $BaTiO_3$ at sintered temperature [15].

1. Dissolution of $BaTiO_3$

$$BaTiO_3 + \text{Mn-Si-O glass} \rightarrow Ba_{0.06}Ti_{0.03}Mn_{0.19}Si_{0.30}O_x \quad (3)$$

2. Crystallization of $Ba_2TiSi_2O_8$

$$Ba_{0.06}Ti_{0.03}Mn_{0.19}Si_{0.30}O_x \rightarrow Ba\left(Ti^{4+}{}_{1-x}Mn^{2+}{}_x\right)O_{3-x} + Ba_2TiSi_2O_8 + Ba_2Ti_9O_{20} \quad (4)$$

There are no Ti rich crystal phases, however, found in this study. Residual Ti ions maybe segregate at the grain boundary of $BaTiO_3$ grains [19]. The segregation of Ti ions at grain boundary may also help to retard grain boundary movement at temperature lower than 1300°C.

4.2 Effects of microstructures on dielectric properties

Dielectric properties closely relate to microstructural characteristics of $BaTiO_3$ materials [20]. Dielectric constant of $BaTiO_3$ is reduced by lower sintered density, smaller grain size (<0.8 μm), smaller tetragonality (c/a≤1.004), second phase, and unfavorable doping elements. A dielectric material with 5% porosity shows considerable reduction on dielectric performance. Second phase composed of $Ba_2TiSi_2O_8$ with low dielectric constant occupies only few volume percents (~2 vol%) in BT disks, and contributes negative effect on dielectric constant as well. Besides that, other factors, grain size and tetragonality of BT, are significant, and dominate the performance of dielectric properties [21].

Grain size of $BaTiO_3$ in 0.7–1.0 μm range has a maximum dielectric constant at room temperature [20]. The constant greatly reduces with the grain size of $BaTiO_3$ either larger or smaller than the specified values (0.7–1.0 μm). As shown in Fig. 10(a), the grain size (2.1 μm) of 0.1 wt% glass-added $BaTiO_3$ was able to get good k value (2300) comparing to the non-glass added sample. However, due to similar grain size (430 nm) of the $BaTiO_3$ in 0.2~3.0 wt% glass-added samples, poor tetragonality degrades the performance of k from 1000 to 500.

Normally, dielectric loss is profoundly affected by the resistivity of sintered $BaTiO_3$. The higher resistivity means difficult transport of electron through the material, in other words, well reduces electron-conduction loss in $BaTiO_3$ capacitor. Mn ion is well known as an acceptor as dopant into $BaTiO_3$, implying an effective electron trapping as Mn is incorporated in $BaTiO_3$ lattice [22]. Therefore, $BaTiO_3$ with <0.5 wt% glass (low Mn-dopant) has smaller dielectric loss, as shown in Fig. 11. However, when the doping level of Mn goes over the solubility limit of Mn in $BaTiO_3$, the residual Mn ion probably forms a second phase [$Mn_2(Ba_xTi_{1-x})O_4$] [15], which can be found as a Mn-rich phase at grain boundaries by Back-Scattering-Electron (BSE) image. Some of secondary phases, including $Mn_2(Ba_xTi_{1-x})O_4$ and $Ba_2TiSi_2O_8$ formed during sintering, would degrade the dielectric loss [23]. Therefore, when the glass addition exceeding a critical amount, more second phases would appear and lead to obvious dielectric loss.

5 Conclusion

Several advantages of adding Mn-Si-O glass for the sintering of BT are investigated in this study. Dissolution of $BaTiO_3$ in the glassy phase helps the formation of low-melting liquid, which performs good-wetting during sintered process. The onset sintered temperature is lowered accordingly.

With solid solution of Mn ion into $BaTiO_3$ grains at higher temperature, second phase ($Ba_2TiSi_2O_8$) also forms at triple junction, acting as grain growth inhibitor. Abnormal grain growth of $BaTiO_3$ is inhibited. as sintered at ≤1275°C.

Dielectric constants of sintered samples are greatly influenced by grain size and tetragonality of sintered $BaTiO_3$. The sample with grain size of 0.7–1.0 μm has higher dielectric constant. For glass-added samples with the same grain size, the higher tetragonality of $BaTiO_3$ would lead to a larger dielectric constant. Dielectric loss is controlled by the solid solution of Mn content into $BaTiO_3$ and the newly formed second phases, including $Mn_2(Ba_xTi_{1-x})O_4$ and $Ba_2TiSi_2O_8$.

Acknowledgement The authors like to thanks the funding partially from the National Science Council in Taiwan and from the Ministry of Economic Affairs, Taiwan, R.O.C. under contract numbers NSC94-2216-E-002-020 and 97-EC-1-A-08-S1-107, respectively.

References

1. S. Sumita, M. Ikeda, Y. Nakano, K. Nishiyama, T. Nomura, Degradation of multilayer ceramic capacitors with nickel electrodes. J. Am. Ceram. Soc. **74**(ll), 2739–46 (1991)
2. C.A. Randall, S.F. Wang, D. Laubscher, J.P. Dougherty, W. Huebner, Structure property relationship in core-shell $BaTiO_3$-LiF ceramics. J. Mater. Res. **8**(4), 871–9 (1993)

3. L. Zhou, Z. Jiang, S. Zhang, Electrical properties of $Sr_{0.7}Ba_{0.3}TiO_3$ ceramics doped with Nb_2O_5, $3Li_2O$-$2SiO_2$, and Bi_2O_3. J. Am. Ceram. Soc. **74**(11), 2925–7 (1991)
4. R.Z. Chen, A. Cui, X.H. Wang, Z.L. Gui, L.T. Li, Structure, sintering behavior and dielectric properties of silica-coated $BaTiO_3$. Mater. Lett. **54**, 314–7 (2002)
5. M. Valant, D. Suvorov, R.C. Pullar, K. Sarma, N.M. Alford, A mechanism for low-temperature sintering. J. Europ. Ceram. Soc. **26**, 2777–83 (2006)
6. C. Metzmacher, K. Albertsen, Microstructural investigations of Barium Titanate-Based Material for base metal electrode ceramic multilayer capacitor. J. Am. Ceram. Soc. **84**(4), 821–6 (2001)
7. Q. Feng, C.J. McConville, D.D. Edwards, Effect of oxygen partial pressure on the dielectric properties and microstructures of cofired base-metal- electrode multilayer ceramic capacitors. J. Am. Ceram. Soc. **89**(3), 894–901 (2006)
8. D.F. Hennings, Dielectric materials for sintering in reducing atmospheres. J. Euro. Ceram. Soc. **21**, 1637–42 (2001)
9. M.R. Opitz, K. Albetsen, J.J. Beeson, D.F. Hennings, J.L. Routbort, C.A. Randall, Kinetic process of reoxidation of base metal technology $BaTiO_3$-based multilayer capacitors. J. Am. Ceram. Soc. **86**(11), 1879–84 (2003)
10. Y.S. Jung, E.S. Na, U. Paik, J. Lee, J. Kim, A study on the phase transition and characteristics of rare earth elements doped $BaTiO_3$. Mater Res Bull **37**, 1633–40 (2002)
11. S. Wang, S. Zhang, X. Zhou, B. Li, Z. Chen, Investigation on dielectric properties of $BaTiO_3$ co-doped with Ni and Nb. Mater. Lett. **60**, 909–11 (2006)
12. S. Wang, S. Zhang, X. Zhou, B. Li, Z. Chen, Influence of sintering atmosphere on the microstructure and electrical properties of $BaTiO_3$-based X8R materials. J. Mater. Sci. **41**, 1813–7 (2006)
13. C.S. Chen, C.C. Chou, I.N. Lin, Microstructure of X7R type base-metal-electroded $BaTiO_3$ capacitor materials prepared by duplex-structured process. J. Europ. Ceram. Soc. **25**, 2743–7 (2005)
14. Y. Mizuno, T. Hagiwara, H. Kishi, Microstructural design of dielectrics for Ni-MLCC with ultra-thin active layers. J. Ceram. Soc. Japan **115**(6), 360–4 (2007)
15. J.C.C. Lin, W.C.J. Wei, Melting and interface reaction of Mn-Si-O glass on $BaTiO_3$. J. Am. Ceram. Soc. **92**(9), 1926–33 (2009)
16. N. Louet, H. Reveron, G. Fantozzi, Sintering behaviour and microstructural evolution of ultrapure-alumina containing low amounts of SiO_2. J. Europ. Ceram. Soc. **28**, 205–15 (2008)
17. M.F. Yan, R.M. Cannon, H.K. Bower, in *Ceramic Microstructures '76*, ed. by R.M. Fulrath, J.A. Pask (Westview, Boulder, 1977), pp. 276–307
18. C.J. Lin, W.C.J. Wei, Grain boundary pinning of polycrystalline Al_2O_3 by Mo inclusions. Mater. Chem. & Phys. **111**, 82–6 (2008)
19. S.B. Lee, W. Sigle, M. Ruhle, Investigation of grain boundaries in abnormal grain growth structure of TiO_2- excess $BaTiO_3$ by TEM and EELs analysis. Acta Mater. **50**, 2151–62 (2002)
20. G. Arlt, D. Hennings, G. de With, Dielectric properties of fine-grained barium titanate ceramics. J. Appl. Phys. **58**, 1619–25 (1985)
21. A. Halliyal, A.S. Bhalla, S.A. Markgraf, L.E. Cross, R.E. Newnham, Unusual pyroelectric and piezoelectric properties of fresnoite ($Ba_2TiSi_2O_8$) single crystal and polar glass-ceramics. Ferroelectrics **62**(1), 27–38 (1985)
22. X. Wang, M. Gu, B. Yang, S. Zhu, W. Cao, Hall effect and dielectric properties of Mn-doped barium titanate. Microelectron. Eng. **66**, 855–9 (2003)
23. M.A. Zubair, C. Leach, The influence of cooling rate and SiO_2 additions on the grain boundary structure of Mn-doped PTC thermistor. J. Europ. Ceram. Soc. **28**, 1845–55 (2008)